Open Access
Volume 6 Issue 3
Research Article

Journal of Water Engineering and Management
ISSN: 2582-6298

Application of Multi-Criteria Decision Analysis Technique for Flood Susceptibility Mapping in an Urban Watershed of Bagmati Basin, Nepal

Suman Hada[1], Pratik Singh Thakuri[2]

[1]Nepal Engineering College, Center for Postgraduate Studies, Prayagpokhari, Lalitpur Nepal
[2]Department of Geosciences, University of Rhode Island, Kingston 02281, Rhode Island, USA

Article Info

Article History:
Received on: October 29, 2025
Revised on: November 10, 2025
Accepted on: December 3, 2025
Published on: December 31, 2025.
Published by Academic Hope

***Corresponding author**: Suman Hada
Email: sumanhd19@gmail.com

How to Cite:
Hada, S. and Thakuri, P. S. 2025. Application of Multi-Criteria Decision Analysis Technique for Flood Susceptibility Mapping in an Urban Watershed of Bagmati Basin, Nepal. Journal of Water Engineering and Management, 6(3):25-38. DOI: https://doi.org/10.47884/jweam.v6i3pp25-38

Abstract

Bagmati Basin within Kathmandu Valley possess the challenge of reoccurring floods mainly in the urban and peri-urban areas. Hanumante watershed, a northeastern tributary of the Bagmati basin in the Kathmandu Valley, is a typical case for urban/peri-urban flooding. Significant recent flood events in the Hanumante Watershed occurred in 2015, 2018, and 2023. Flood assessments in Nepal have traditionally relied on hydraulic models combined with statistical extrapolation of flood discharge. Whereas, this research evaluates the use and utilization of Multi-Criteria Decision Analysis (MCDA) for GIS-based flood mapping. The framework of this study is both innovative and robust, utilizing a unique two-tier MCDA process, with results validated against two different sets of ground-level data. Flood hazard susceptibility was mapped using the Analytical Hierarchy Process (AHP) method, considering 15 parameters categorized under 4 (four) criteria namely Hydro-meteorological, Morphological, Soil-permeability, and Land use-land cover (LULC) dynamics. The flood susceptibility map, was validated with the 1-D analysis of Hydrologic Engineering Centre's River Analysis System (HEC-RAS) model, a flood benchmarking survey data of the area, achieving an Area Under the Receiver Operating Curve (AUC) >90. Furthermore, the map was verified with georeferenced ground level photographs of Hanumante Flood 2023, demonstrating the accuracy and applicability of the proposed framework of this elaborated study. The resultant flood susceptibility map offers crucial and evident insights for genuine policymakers and structured planners to enhance flood resilience in the Hanumante Watershed. Similarly, the parameters and the proposed framework of this elaborated study can be replicated to other urban/peri-urban watersheds of the similar nature.

Keywords: Urban Flood: MCDA: AHP: HEC-RAS: AUC: Flood Hazard.

Introduction

Nepal ranks twentieth worldwide in terms of flood-affected population Factors such as rugged and rashed topography, weak and cracky geological formations, occasional timebound glacial lake outbursts, concentrated and scarced monsoon rainfall, and specific land utilization and usage practices contribute to environmental challenges in the area (Winsemius and Ward, 2015). Some of the major devastating flood events that took place in Nepal are: the 1993 floods in Central Nepal, the 1998 Rohini River and other Terai flood, the 2008 Koshi embankment breach flood, the 2008 floods in Far-West Nepal, Seti Flood in 2012, 2013, 2014 and 2017 flood events in the mid and far western region, Glacial Lake outburst floods: Bhote Koshi, 2016 and Barun Khola, 2017, Melamchi flood on June 14, 2021. Flood events between 1954 and 2018 caused 7,599 deaths affecting 6.1 million people, causing economic loss of 10.6 billion USD with an average loss and

losing of life being 100 people annually (Shrestha et al., 2020). There are several tools and techniques to map and assess the flood risk. Among these, modelling and simulation: hydrological, hydraulic and hydrodynamic are widely used featuring 24% of total articles in flood-related research globally. Similarly, statistical analysis is another popular method with a 20% stake in the published article in the field. However, only 6% of total articles have employed evaluation-based and observatory methodologies that consisted of framework designated proposals, transparent reviews and pre-post-flood assessments, having theoretical aspects (Diaconu et al., 2021). A framework combining hydraulic/ hydrological model and curative remote sensing data in a GIS environment produces the best result when detailed flood hazard mapping and flood risk assessment are required (Adjei-Darko, 2017).

MCDA is a technic used to choose an alternative based on predefined criteria, which may be either qualitative or quantitative. This approach has proven effective in evaluating real-world situations where a well-supported decision among multiple options is required (Kumar, 2010). These methods serve as a support tool, capable of comprehensively analyzing and addressing technological, ecological, and social aspects within complex decision scenarios (Ogato et al., 2020). The most widely adopted methods of MCDA are AHP, ANP, DEA, WSM, WPM, and GP. Among them, AHP has gained widespread use across diverse applications worldwide due to its simplicity and adaptability (Ho, 2008). Floods in the Hanumante River have frequently affected three municipalities: Bhaktapur, Madhyapur Thimi, and Suryabinayak (Bhatta and Pandey, 2020). Bhaktapur is one of the municipalities in Nepal, where flooding has emerged as a significant issue. The largest floods on record within the decade in Bhaktapur occurred on August 27, 2015, July 12, 2018 and August 8, 2023 (Pradhanand Pokharel, 2017). Therefore, it has been felt that the application of the MCDA techniques would be the evidence-based approach for mapping flood susceptibility. Previous research on flood mapping with MCDA-AHP techniques adopts the process of pair-wise discrete comparison of all the selected parameters in a single-step (Swain et al., 2020; Parsian et al., 2021; Chaulagain et al., 2023; Mokhtari et al., 2023). This study proposes a distinctive and robust framework for the MCDA-AHP technique by implementing a two-tier pairwise comparison process, one within the parameters and another within the criteria, and validating the resultant flood susceptibility map with multiple ground-level data. The proposed farm work upon the successful application of the flood-prone watershed of Hanumante, can be scaled in other watersheds of similar nature.

Materials and Methods

Description of Study Area

Hanumante, a tributary of the Bagmati River is an 8th-order river as per Strahler's stream ordering done using the digitized contour data from the Department of Survey, Nepal. It has a catchment area of 141.83 km^2 and a confluence with the Manohara River (Fig. 1). It is an ungauged river hydrologically however, four meteorological stations namely, Nagarkot (1043), Bhaktapur (1052), Changunarayan (1059), and Nangkhel (1082) are installed within the watershe(Fig.1). Hamumante watershed is comprised of Bhaktapur (ward no. 1 to 10), Changunarayan (ward no. 1 to 9), Madhyapur Thimi (ward no. 1 to 9) and Suryabinayak Municipality (ward no. 1 to 10) of Bhaktapur district, Godawari (ward no.1,2,3,14), Lalitpur Metropolitan City (ward no. 29) and Mahalaxmi Municipality (ward no. 5 to 10) of Lalitpur district.

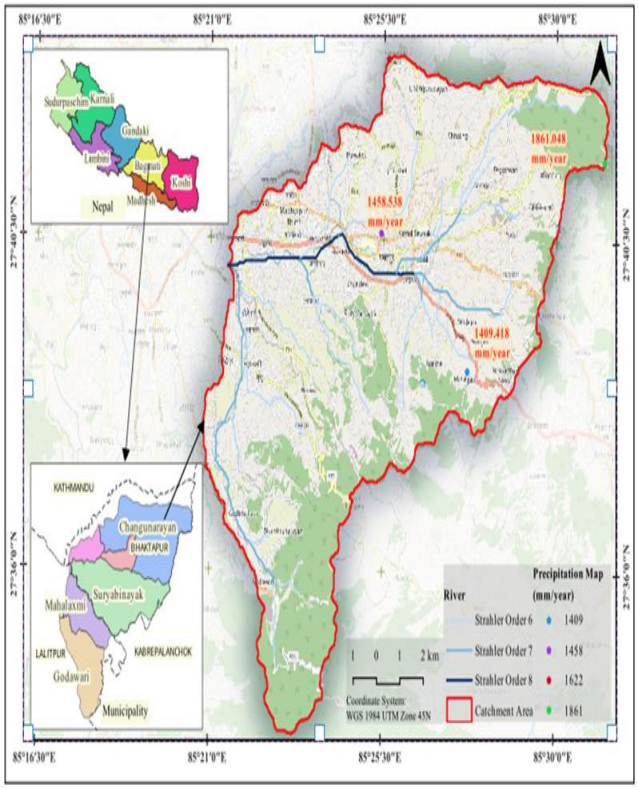

Fig. 1 Study area of the Hanumante Watershed

Table 1 Specification of data used for the research

Data Type	Spatial Resolution	Source
DEM	30m x 30m	Produced from 20 m interval contour of sheet 102 and 157, Survey Department
Precipitation	Station-wise data	Department of Hydrology and Meteorology (DHM)
SND	30m x 30m	Produced from DEM
Stream Power Index (SPI)	30m x 30m	Produced from DEM
Slope (degree)	30m × 30m	Produced from DEM
Topography (Landform)	30m × 30m	Global ALOS Landforms, USGS/ Google Earth Engine
Topographic Ruggedness Index (TRI)	30m ×30m	Produced from DEM
Proximity to River	30m × 30m	Produced from DEM
LANDSAT 8	30m × 30m	USGS, Date of acquisition: 2015-10-07- 2020-09-08
Soil Moisture Index (SMI)	30m × 30m	Produced from Landsat 8
Topographic Wetness Index (TWI)	30m × 30m	Produced from Slope/DEM
Soil Erodibility Factor(K) (RUSLE Based)	30m ×30m	Produced from National Soil Science Research Centre (NARC), web portal: https://soil.narc.gov.np/soil/soilmap/
Rainfall Erosivity(R) Factor (RUSLE Based)	30m × 30m	Produced using precipitation data from DHM
LULC Classes	30m × 30m	https://doi.org/10.26066/RDS.1972729
Normalized Difference Vegetative Index (NDVI)	30m × 30m	Produced from Landsat 8 images
Topographic survey data	AutoCAD, Excel	Pre-Construction Survey Data of Hanumante Interceptor, Construction of Intercepting Sewerage System in Hanumante River (IS01) (PID, 2016)

Source of Data

Primary data collection included collection of the flood depth-extent data through a flood benchmarking survey at the flood plains of Hanumante River, whereas open-source data and secondary information from different published and unpublished documents, government web portals and other relevant websites were collected (Table 1).

Flood Susceptibility Parameters

Fifteen parameters, critical to causing flood were selected and grouped into three criteria as a) Hydro-meteorological: Precipitation, SND and SPI, b) Morphological: Elevation, Slope, Topography, TRI and Proximity to the river, c) Soil-permeability: SMI, TWI, Soil Erodibility Factor and Rainfall Erodibility Factor, and d) LULC Dynamics: LULC, NDVI and SAVI, based on literature reviewed (Swain et al., 2020) and relevancy in the study area. Processing of parameter data, generation of the base layer in raster form with defined spatial resolution, and re-classification of base layers into five susceptibility classes was done (Fig.2).

Hydro-meteorological Criteria

The hydro meteorological criteria are comprised of parameters namely Precipitation, Stream Network Density and Stream Power Index. Four meteorological stations(Table 2) contained within the watershed were considered following the adequacy of the required number of stations (IS 4987, 1994).Precipitation data from 2000 to 2018, obtained from the DHM, was used to compute the average annual precipitation (mm/year) (Fig. **3**). The Kriging interpolation method was then applied to generate a precipitation map for the study area.

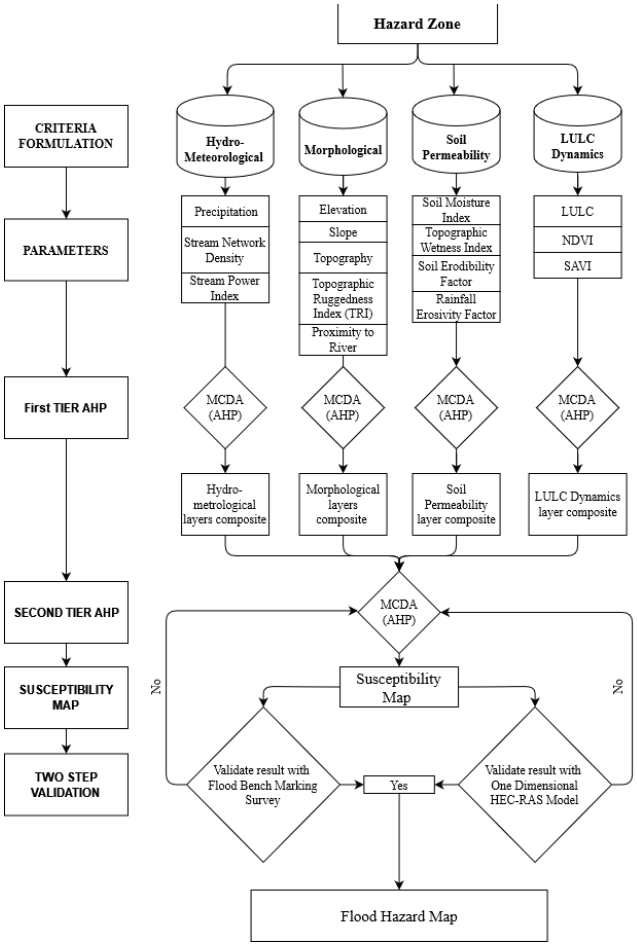

Fig. 2 Methodological framework for flood susceptibility mapping

Table 2 Rain gauge stations within the Hanumante Watershed

Name	Latitude	Longitude	Average Annual Precipitation	Maximum Rainfall (mm/day)
Nagarkot (1043)	27.693342	85.520858	1841	179
Bhaktapur (1052)	27.676680	85.423969	1458	260
Changunarayan (1059)	27.716058	85.426755	1622	165
Nangkhel (1082)	27.645725	85.461583	1409	191

SND which is generally understood as the ratio of the total length of the stream network to the watershed area was generated using the Line Density tool available in QGIS (Swain et al., 2020). The Stream Power Index (SPI), a hydrological metric that describes the erosive power of flowing water in a watershed was calculated based on the slope (Bachri et al., 2019). The associated mathematical formulation of SPI is as given in the Equ. 1,

$$SPI = FlowAccumulation \times CellSize \times \tan(Slope \times 0.017453) \quad (1)$$

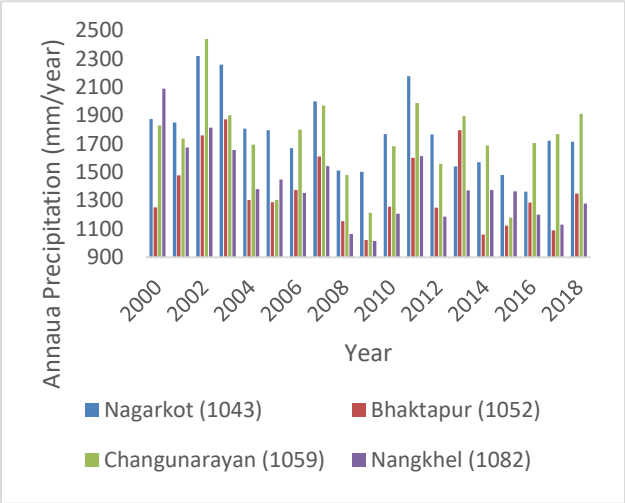

Fig. 3 Annual precipitation data of stations within the Hanumante Watershed

Morphological Criteria

Elevation, slope (degree), topography, topographic ruggedness index and proximity to the river are grouped under morphological criteria. DEM with 30m resolution was generated from 20 m interval contour of sheets 102 and 157, issued by the Department of Survey, Government of Nepal. Parameters such as Elevation and slope were directly generated from DEM. The topography map was extracted from Global ALOS Landforms using GEE. Similarly, the Proximity to the river was computed through the Euclidean distance method. The Topographic Ruggedness Index (TRI), is a measure of ruggedness or variability of the terrain considering the difference in the elevation between adjacent cells of DEM (Drobot, 2007), calculated and evaluated using the Equ. 2.

$$T.R.I. = (Z_{max} - Z_{min})/\sqrt{A} \quad (2)$$

Z_{max} = Maximum elevation;
Z_{min} = Minimum elevation;
A = Catchment area in km²

Soil Permeability Criteria

Under the Soil Permeability Criteria, following parameters are included: SMI, TWI, Soil Erodibility Factor and Rainfall Erodibility Factor. SMI is a metric used to quantify soil moisture levels relative to its capacity to hold water. It is mathematically defined as the ratio of the difference between the current soil moisture and the permanent wilting point to the difference between field capacity and residual soil moisture. The SMI values range on the scale of 0 to 1, where 0 represents extremely dry conditions and 1 represents extremely wet conditions (Saha et al., 2018). The soil moisture index layer was generated by analyzing LANDSAT-8 satellite images. The Topographic Wetness Index (TWI) quantifies and presents clearly the spatial distribution of soil moisture based on topography. The equation used to calculate TWI is provided in Equ. 3.

$$\mathrm{TWI} = \ln\left(\frac{a}{\tan b}\right) \quad (3)$$

a =cumulative upslope draining area per unit contour length;
b = local slope at the point of contact.

Soil Erodibility Factor (K) is an integral parameter of the (RUSLE), that is used to Evaluate soil erosion rates. K quantifies the ease with which soil can be detached and transported by surface runoff (Dahal, 2020). The mathematical formulation for computing the K is provided in Equations 4-8.

$$\mathrm{Kusle} = (f_{sand} \times f_{silt} \times f_{clay} \times f_{orgc} \times 0.1317) \quad (4)$$

Where,

$$f_{Sand} = \left[0.2 + 0.3 \times \exp\left(-0.256 \times m_{Sand}\left(1 - \frac{m_{Silt}}{100}\right)\right)\right] \quad (5)$$

$$f_{Clay} = \left(\frac{m_{Silt}}{m_{Clay}+m_{Silt}}\right)^{0.3} \quad (6)$$

$$f_{OrgC} = \left(1 - \frac{0.25*m_{OrgC}}{m_{OrgC}+\exp[3.72-2.95*m_{OrgC}]}\right) \quad (7)$$

$$f_{Silt} = \left(1 - \frac{0.7\left(1-\frac{m_{Sand}}{100}\right)}{\left(1-\frac{m_{Sand}}{100}\right)+\exp\left[-5.51+22.9*\left(1-\frac{m_{Sand}}{100}\right)\right]}\right) \quad (8)$$

m_{OrgC} =% of organic matter
m_{Sand} =% of sand content
m_{Silt} =% of silt content
m_{Clay} =% of clay content

The soil maps from NARC were used and analyzed to generate the Soil Erodibility Factor map. Similarly, the Rainfall Erodibility Factor (R) is another integral parameter of the (RUSLE) which measures the impact of rainfall on soil erosion. R quantifies the effect of rainfall-runoff on soil erosion considering the intensity and volume of the rainfall. (koirala et al.,2019). K can be calculated based on the formula provided in Equ. 9.

$$R = 38.5 + 0.35P \quad (9)$$

R = Rainfall Erosivity Factor.
P = Average annual rainfall (mm/year).

LULC Dynamics

LULC classes, NDVI and SAVI are grouped in LULC dynamics. The NDVI layer, which quantifies the vegetation health and density based on satellite imageries was developed by processing Band 5- Near Infrared (NIR) and Band 4-Red of LANDSAT-8 image. Equation 10 can be used to compute the NDVI,

$$\mathrm{NDVI} = \frac{\mathrm{NIR}-\mathrm{Red}}{\mathrm{NIR}-\mathrm{Red}} \quad (10)$$

NDVI value ranges from -1 to 1, where negative values represent water, snow and cloud, NDVI value between 0.2 and 0.4 represents barren land, built-up area and rock; 0.4 to 0.6 represents moderate vegetation, while 0.6 to 1 represents dense vegetation cover (Alex and Ramesh, 2017). Soil-Adjusted Vegetative Index (SAVI) is the improvement over NDVI by reducing soil background effects, by using the soil brightness correction factor (Huete, 1988). SAVI is calculated using the equation,

$$\mathrm{SAVI} = \left(\frac{\mathrm{NIR}-\mathrm{Red}}{\mathrm{NIR}+\mathrm{Red}+L}\right)(1+L) \quad (11)$$

NIR= Near Infrared Band 5 of LANDSAT image
Red= Red Band 4 of LANDSAT image
L= Amount of green vegetation cover

For areas with no vegetation, L=1; moderate green vegetation cover, L=0.5 and very high vegetation cover, L=0. SAVI value ranges from -1 to 1. With selected flood susceptibility parameters, the parameter maps were created by processing in a GIS environment and re-classified into five susceptibility classes using the Natural Break, Jenks method (Table 3). Parameters in various criteria listed and elaborated in this section is well depicted in Fig. 4.

Table 3 Flood susceptibility class ranges and rating

Parameters	Unit	Influence	Re-classification Method	Very High (5)	High (4)	Moderate (3)	Low (2)	Very Low (1)
Hydro-meteorological								
Precipitation	mm/year	Positive	Natural Jenks	1735.71 - 1860.80	1644.09 - 1735.71	1568.33 - 1644.09	1497.85 - 1568.33	1409.76-1497.85
Stream Network Density	m/m	Positive	Natural Jenks	0.0044-0.0071	0.0030-0.0044	0.0017-0.0030	0.0005-0.0017	0-0.0005
Stream Power Index	level	Positive	Natural Jenks	47361603-103628808	21454401-47361603	7691200-21454401	1619200-7691200	0.054-1619200
Morphological								
Elevation	m	Negative	Manual	1276-1305	1305-1320	1320-1330	1330-1375	1375-2680
Slope	Degree	Negative	Manual	0-15	15-25	25-35	35-45	45-60
Topography	Level	Positive	Grid Value	34-42	24-34	15-24	13-15	11-13
Topographic Ruggedness Index	Level	Negative	Natural Jenks	0-2.2	2.2-6.1	6.1-10.7	10.7-15.7	15.7-36.7
Proximity to River	m	Negative	Manual	0-200	200-300	300-400	400-1000	1000-2783
Soil-permeability								
Soil Moisture Index	Level	Positive	Natural Jenks	0.59-1	0.45-0.59	0.35-0.45	0.26-0.35	0-0.26
Topographic Wetness Index	Level	Positive	Natural Jenks	19-27.50	15-19	12-15	10-12	7.45-10
Soil Erodibility Factor	Level	Positive	Natural Jenks	0.030302 - 0.03439	0.028223 - 0.030302	0.026194 - 0.028223	0.022893 - 0.026194	0.017073 - 0.022893
Rainfall Erodibility Factor	Level	Positive	Natural Jenks	646-683	620-646	595-620	572-595	540-572
LULC dynamics								
Land Cover (2019)	Level	Negative	Grid Value	Water Body, Build Up Area (1,6)	Cropland (7)	Grassland (10)	Forest, Other Woodland (4,11)	Bare Rock
NDVI	Level	Negative	Natural Jenks	-0.0491-0.1891	0.1891-0.2795	0.2795-0.344	0.344-0.3999	0.39993-0.5931
SAVI	Level	Negative	Natural Jenks	-0.07-0.28	0.28-0.41	0.41-0.51	0.51-0.60	Very Low

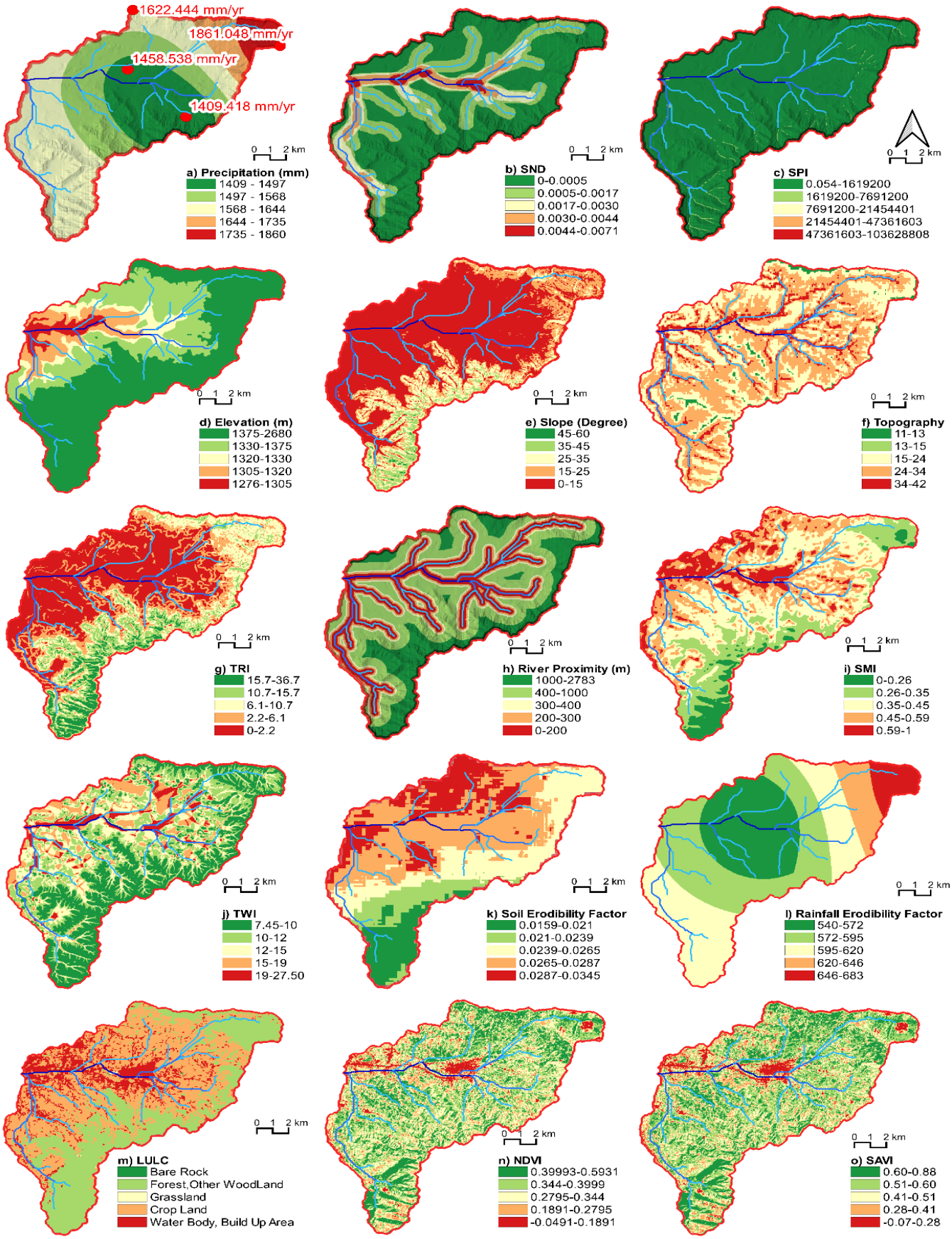

Fig. 4 Flood susceptibility parameter maps

Application of AHP for Assigning Weights

The AHP was applied to rank the parameters systematically by conducting pairwise comparisons. The standard pairwise ranking scale (Saaty, 1977) is presented in Table 4. The weightage factor was then calculated and validated using a Consistency Ratio (CR) (Saaty, 1977), which should be less than 0.1 (Saaty et al., 2001). The equation formulated to compute the consistency ratio is provided in Equ. (12).

Table 4 Saaty's pairwise comparison scale

Rating	Description
1-Equal	Both alternatives have equal importance.
3-Moderate	One of the alternatives is slightly more important than the other one.
5-Strong	One of the alternatives is strongly more important than the other one.
7-Very Strong	One of the alternatives is very strongly important compared to the other one.
9-Extreme Importance	One of the alternatives is strictly superior to the other one.

$$CR = \frac{\text{CI}}{\text{RI}} \quad (12)$$

$$\text{CI} = \frac{(\lambda_{max} - \text{n})}{\text{n}-1} \quad (13)$$

Where,
CR= Consistency Ratio
CI= Consistency Index
n= number of parameters
RI= random index depending upon number of parameters (Saaty, 1977) as indicated in Table 5

Table 5 Saaty's Random Index

Number of Factor	1	2	3	4	5	6	7	8	9
RI	0	0	0.58	0.9	1.12	1.24	1.32	1.41	1.45

Generally, pair-wise comparison is carried out directly between all available parameters. However, when comparing a large number of parameters, direct pair-wise comparison can become impractical. As the number of parameters increases, the complexity of making meaningful comparisons also increases proportionally. Consequently, it becomes difficult to maintain consistency and relevance across all comparisons, leading to potential issues of incomparability. To address this problem, a unique approach of hierarchical structuring is adopted in this study.

The overall set of parameters is broken down into criteria or categories. The first tier of comparison is conducted within the parameters of the same criteria, while the second tier compares the criteria themselves. By adopting this approach, it is assumed that cognitive bias in comparison is reduced, making the comparisons more logical. In the first tier, the weightage for parameters was derived based on a pairwise comparison of parameters in individual criteria namely Hydro-meteorological, Morphological, soil-permeability and LULC dynamics**.** Experts with depth knowledge were requested to assign the weights in Satty's scale of 1-9, for the pairwise comparison. Further, the weightage was optimized by checking the requirement of consistency ratio value to be less than 0.1 (Saaty, 1977). Criteria maps were then generated through the weighted overlay method applying the weightage of each parameter derived through AHP. As such, in the second tier, the same process of pairwise comparison through expert judgement was repeated but for the criteria itself rather than their underlying parameters as shown in Table 7.

Validation of Flood Susceptibility Map

The flood susceptibility map was validated using the Area under the Receiver Operating Characteristics (ROC) curve (AUC) method (Abeysiriwardana et al., 2022). ROC is the plot of True Positive Rate (TPR) as a function of False Positive Rate (FPR) calculated using Equ. (14) and (15).

$$\text{TPR} = \frac{\text{TP}}{\text{TP} + \text{FN}} \quad (14)$$

$$\text{FPR} = \frac{\text{FP}}{\text{TN} + \text{FP}} \quad (15)$$

Where,
TP= True Positive
TN= True Negative
FP= False Positive
FN=False Negative

Table 6 Weightage and consistency ratio for parameters (first tier)

Parameters	Criteria Weight (%)	Consistency Index (CI	Consistency Ratio (CR) %
Hydro-meteorological			
Precipitation	11	0.03	4.77
Stream Network Density	63		
Stream Power Index	26		
Morphological			
Elevation	47	0.09	8.36
Slope	24		
Topography (Landforms)	15		
Topographic Ruggedness	9		
Proximity to River	4		
Soil-permeability			
Soil Moisture Index	56	0.06	6.54
Topographic Wetness Index	26		
Soil Erodibility Factor	12		
Rainfall Erodibility Factor	6		
LULC dynamics			
LULC	63	0.03	4.77
NDVI	26		
SAVI	11		

The model for predicting flood susceptibly performances can be categorized based on AUC values as follows: Average if 0.6 < AUC < 0.7, Good if 0.7 < AUC < 0.8, Very Good if 0.8 < AUC< 0.9 and Excellent if 0.9 < AUC < 1(Al-Juaidi et al., 2018). The very high and high flood susceptibility classes from the susceptibility map are extracted for validation, based on the assumption that if ground-level flood data corresponds with these classes, the susceptibility is confirmed. The testing dataset to generate AUC value was acquired using two approaches, a) flood bench-marking survey and b) Flood hotspots. Flood hotspots are generated by GIS based AI random selection of 20% points from the inundation raster obtained by performing a one-dimensional steady flow analysis using the HEC-RAS model.

HEC-RAS-based One-Dimensional Steady Flow Analysis

One dimensional steady flow hydraulic analysis was carried out in the Hanumante River from the confluence of the Hanumante River and Kasan Khola to the confluence of the Hanumante River and Manohara River (Fig. 5), which is low-lying, rapidly urbanizing and among the most flood affected areas during 2018 flood event (Bhatta and Pandey, 2020). Estimation of flood for different periods (2, 5, 10, 20,50and100years) was done by using regional methods (WECS/DHM, Modified DHM, MHSP) and empirical formula (Fuller's Formula, Modified Dicken's and B.D Richard's), as referred from DoED (2006). The average flood discharge estimated by all the methods was adopted for further computations. The HEC-RAS model was used to develop a one-dimensional steady flow model and to obtain flood depth and extent raster for different return periods. Twenty per cent of randomly selected points through the GIS-based automated algorithm were used to develop a testing dataset. These testing datasets were used to validate the reliability of the flood susceptibility map.

Table 7 Weightage and consistency ratio for criteria (second tier)

Parameters	Criteria Weight (%)	Consistency Index (CI)(%)	Consistency Ratio (CR) %
Hydro-meteorological	31	0.02	2.48
Morphological	49		
Soil-permeability	8		
LULC dynamics	13		

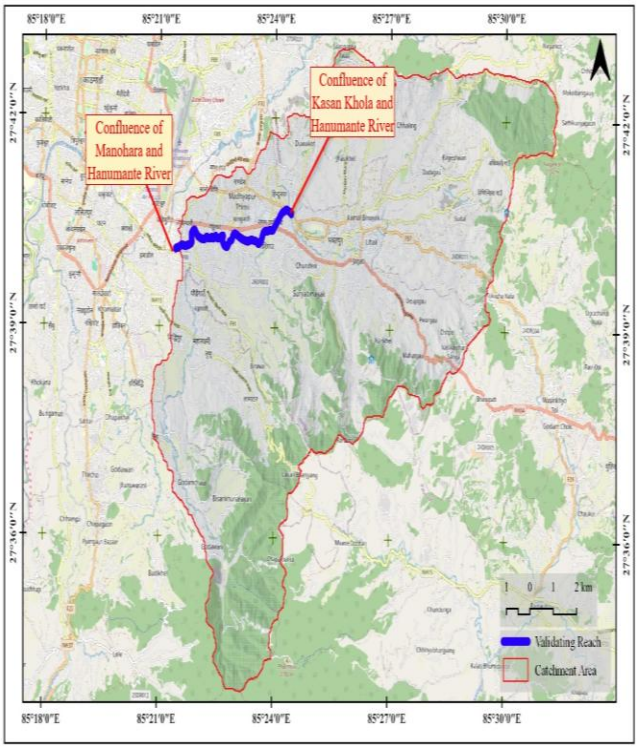

Fig. 5 Validating Reach for One dimensional steady flow analysis.

Flood Bench-Marking Survey

Flood extent and depth were quarried with people who reside within the area or those who were present or were directly affected by the flood in the Hanumante River. Thus, collected geo-referenced flood benchmark data was used to develop the HFL raster using the Triangular Irregular Network (TIN) interpolation method.

Hanumante River Flood 2023

The Hanumante River evidenced significant floods in 2023. The major areas affected by the Hanumante River Flood 2023 were visited and marked using the geo-referenced photograph. Also, the photograph of areas affected by the Hanumante River Flood 2023 was downloaded from the S4W-Nepal portal (S4W-Nepal, 2023). The flood-affected areas were intersected with flood susceptibility map results using the GIS platform just to cross-verify the result of the flood susceptibility map.

Results and Discussion

Flood Susceptibility Mapping

In the hydro-meteorological criteria, the AHP-weightage reflected the highest influence of SND (0.63), followed by SPI (0.26) and precipitation (0.11). Whereas, for the morphological criteria, the order of influence from highest to lowest was proximity to river (0.47), elevation (0.24), topography (0.15), topographic ruggedness index (0.09), and slope (0.04). Similarly, in the case of soil-permeability criteria, average soil moisture had the greatest influence (0.56), followed by the topographic wetness index (0.26), soil erodibility factor (0.12), and rainfall erodibility factor (0.06). Furthermore, the order of influence is LULC (0.63), NDVI (0.26), and SAVI (0.11) for the LULC dynamics criteria. Additionally, the AHP-weightage of criteria layers (Table 7) ranked the influences of the criteria as Morphological (0.49), Hydro-meteorological (0.31), LULC dynamics (0.13), and Soil-permeability (0.08). The maximum eigenvalue (λ max) was 4.07, and the consistency ratio (CR) was 2.48%.

As shown in the flood susceptibility criteria map(Fig.6) the hydro-meteorological criteria map shows very high and high flood susceptibility zones at the confluences of tributaries with the main channel of the Hanumante River. The morphological criteria map identifies high-risk areas within 200 meters of the river across various wards in the same municipalities. The soil-permeability criteria map highlights high flood-risk areas with high soil moisture near the river. The LULC dynamics map points to built-up areas near the river as a susceptibility factor to flooding. The flood susceptibility map (Fig. 7) revealed that very high-risk zones are characterized by the confluences of tributaries with the main channel, lower elevation, valley locations, proximity to the river, and built-up areas with minimal vegetation coverage. The flood susceptibility map classifies the study area into very high, high, moderate and very low susceptibility classes, covering 0.72%, 9.76%, 37.76%, 45.05%, and 6.72% of the area, respectively.

Overall, 10.48% of the area falls into the very high and high susceptibility classes (Fig. **8**). The susceptibility map depicts Ward 4 in Madhyapur Thimi Municipality of Bhaktapur District, and Wards number 7, 1, 8, and 5 of Bhaktapur Municipality are the most flood-prone areas which have the highest coverage of very high susceptibility class.

Validation of Flood Susceptibility Map

To validate the flood susceptibility map, the very high and high susceptibility classes were extracted using a conditional expression in the GIS

environment. The validation process involved calculating the Area under ROC curve (AUC) value with testing datasets generated from a) the One-dimensional HECRAS model (Fig. 9), and b) the flood benchmarking survey (Fig.10). Both methods yielded AUC values greater than 90%, quantitatively indicating a high degree of reliability and the effectiveness of the two-tier AHP-based framework of flood susceptibility mapping adopted for this study (Fig.11).

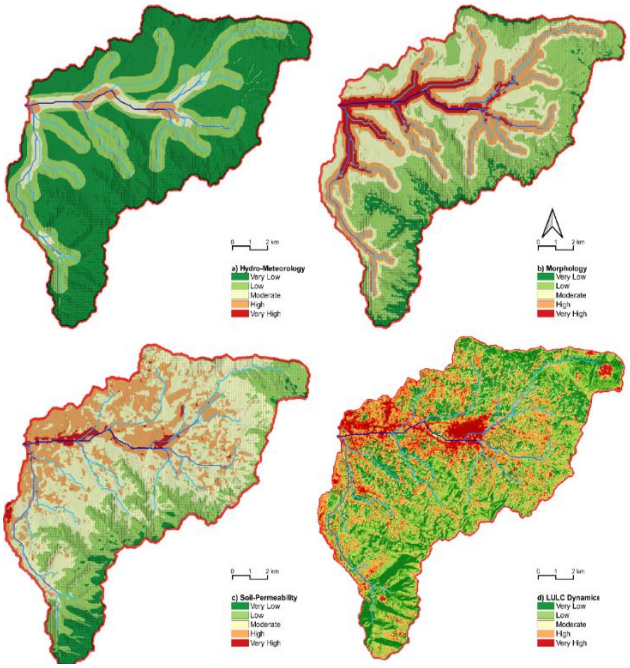

Fig. 6 Flood susceptibility criteria maps

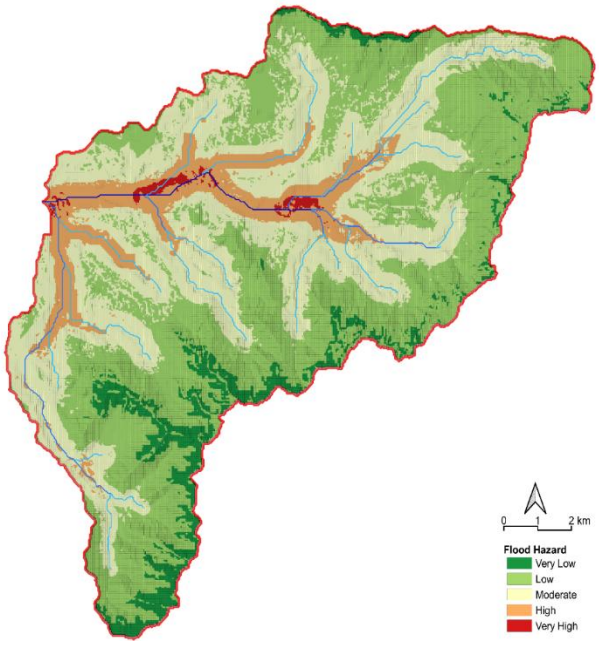

Fig. 7 Flood susceptibility map

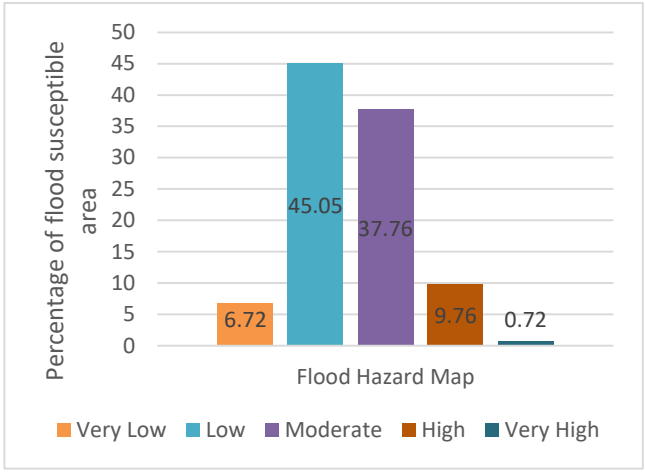

Fig. 8 Percentage of an area susceptible to flood

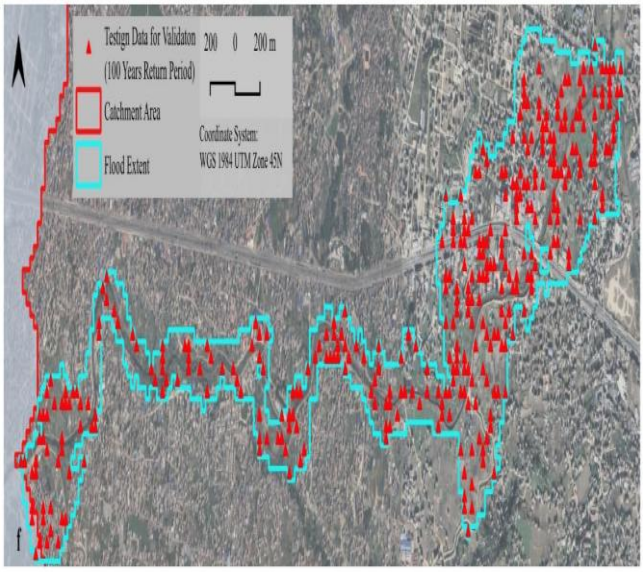

Fig. 9 Twenty percentage random samples from flood extent map of HECRAS analysis (100 years)

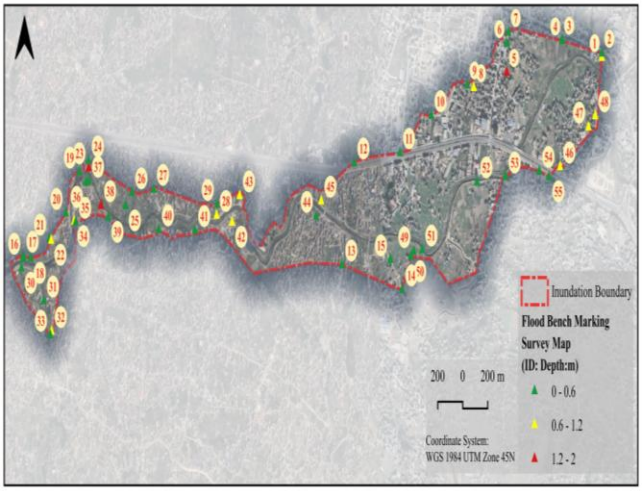

Fig. 10 Flood depth/extent map from flood bench-marking survey

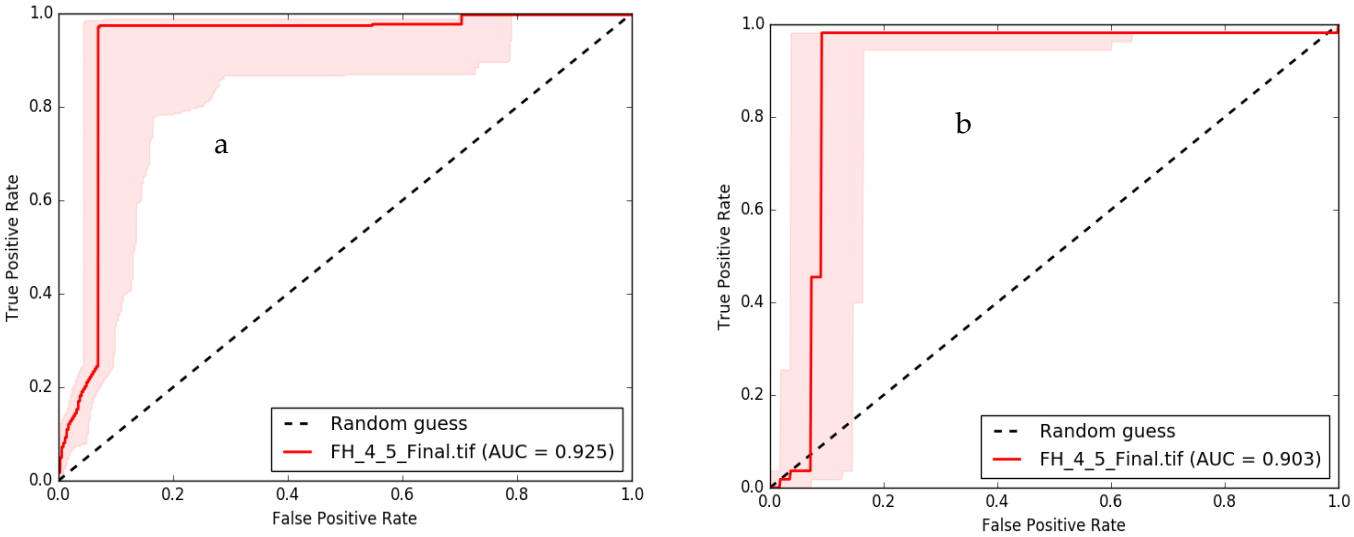

Fig. 11 Validation of flood susceptibility map by AUC using a) HECRAS model and b) flood bench marking survey

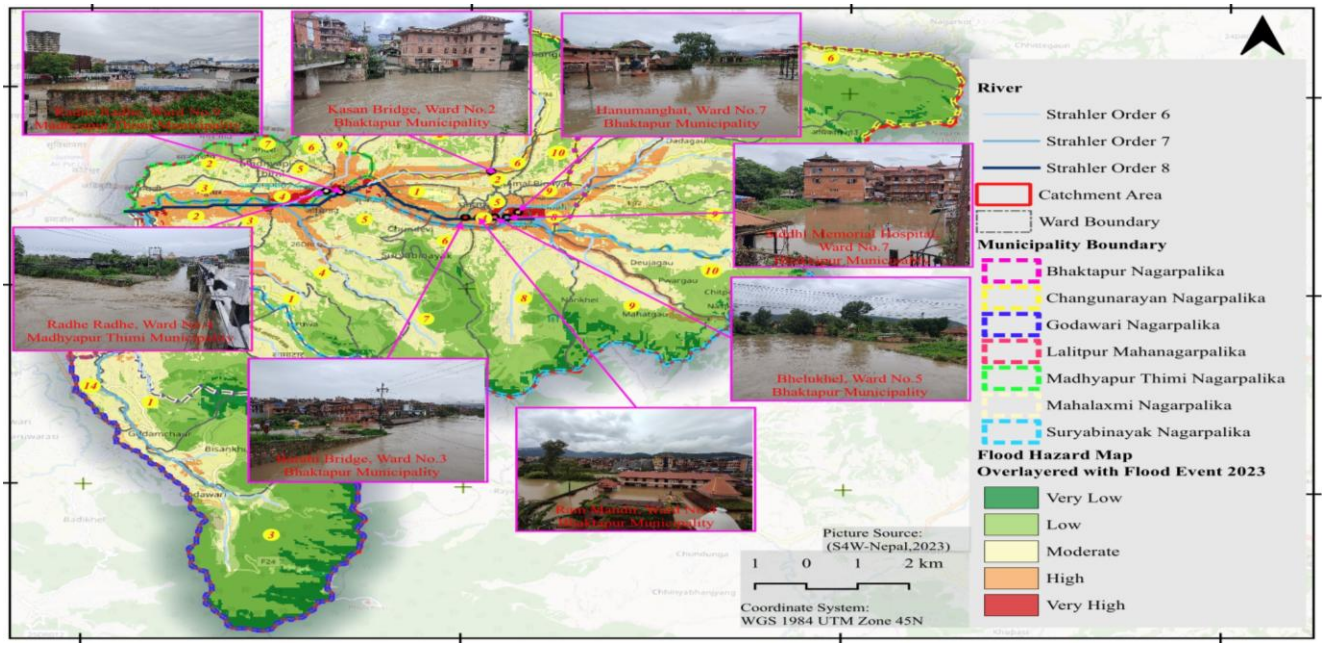

Fig. 12 Hanumante flood event 2023

Hanumante River Flood 2023

The flood event in the Hanumante Watershed on August 8, 2023, significantly impacted Hanumanghat (ward 7), Siddhi Memorial Hospital (ward 7), Bhelukhjel (ward 5), Rammandir (ward 3), Barahisthan (ward 3), and Kasan Khola Bridge in Bhaktapur Municipality, as well as wards 2 and 9 in Madhyapur Thimi Municipality. Upon the cross verification of flood susceptibility map with the georeferenced images of 2023 Hanumante flood event it was found that the map generated as product of this study and especially the high and very high susceptibility class perfectly align with the 2023 Hanumante flood affected areas (Fig. 12).

Conclusions

This study systematically explored and provided the evidence of applicability and reliability of AHP framework of the MCDA technique integrated with GIS for flood susceptibility mapping in the Hanumante Watershed. The map indicated that 10.48% of the area is highly prone to floods, with 99.29% of this area being within 200 meters of the river. The findings of this study can provide crucial insights for policymakers and planners. The flood hazard map can inform flood resilience measures, risk reduction strategies, and land use planning in the watershed. Crucially, the proposed and validated

parameters and the framework of this study set a milestone for flood susceptibility mapping on several other watersheds in the mid-hills of Nepal. As such, it can be concluded that the integration of proposed MCDA farmwork and associated parameters with GIS for flood risk mapping offers a comprehensive and effective approach to identifying flood-prone areas in Nepal, enhancing the ability to predict and mitigate the flood hazards.

Data Availability Statement

The datasets generated during the current study are available from the corresponding author on reasonable request.

Conflict of Interest

The authors declare that they have no known competing financial interests or personal relationships that could have appeared to influence the work reported in this paper.

Funding

This research received no external funding.

Reference

Abeysiriwardana, H. D. and Wijesekera, N. T. S. 2022. Application of GIS and logistic regression for flood susceptibility mapping in Nilwala River Basin, Sri Lanka. Engineer: Journal of the Institution of Engineers, Sri Lanka, 55, 2, 1. https://doi.org/10.4038/engineer.v55i2.7503

Adjei-Darko, P. 2017. Remote sensing and geographic information systems for flood risk mapping and near real-time flooding extent assessment in the Greater Accra Metropolitan Area. http://www.diva-portal.org/smash/record.jsf?pid=diva2%3A1087549

Alex, E. C. and Ramesh, K. V. 2017. Quantification and understanding the observed changes in land cover patterns in Bangalore. International Journal of Civil Engineering and Technology, 8, 4, 597-603. http://www.iaeme.com/IJCIET/index.asp

Al-Juaidi, A. E. M., Nassar, A. M. and Al-Juaidi, O. E. M. 2018. Evaluation of flood susceptibility mapping using logistic regression and GIS conditioning factors. Arabian Journal of Geosciences, 11, 24. https://doi.org/10.1007/s12517-018-4095-0

Bachri, S., et al. 2019. Landslide susceptibility mapping in Kelud Volcano using spatial multi-criteria evaluation. IOP Conference Series: Earth and Environmental Science, 273, 012014. https://doi.org/10.1088/1755-1315/273/1/012014

Bhatta, B. P. and Pandey, R. K. 2020. Bhaktapur urban flood-related disaster risk and strategy after 2018. Journal of APF Command and Staff College,3,1,72-89. https://doi.org/10.3126/japfcsc.v3i1.27530

Chaulagain, D., et al. 2023. Flood susceptibility mapping of Kathmandu Metropolitan City using GIS-based multi-criteria decision analysis. Ecological Indicators, 154, 110653. https://doi.org/10.1016/j.ecolind.2023.110653

Dahal, R. 2020. Soil erosion estimation using RUSLE modeling and geospatial tool: Case study of Kathmandu District, Nepal. Forestry: Journal of Institute of Forestry, Nepal, 17, 118-134. https://doi.org/10.3126/forestry.v17i0.33627

Diaconu, D. C., Costache, R. and Popa, M. C. 2021. An overview of flood risk analysis methods. Water,13,4. https://doi.org/10.3390/w13040474

DoED. 2006. Design guidelines for headworks of hydropower projects. Department of Electricity Development, Nepal.

Drobot, R. 2007. Methodology for determining torrential catchments in which human settlements are exposed to flash floods. Technical University of Civil Engineering, Bucharest.

Ho, W. 2008. Integrated analytic hierarchy process and its applications: A literature review. European Journal of Operational Research, 186, 211-228. https://doi.org/10.1016/j.ejor.2007.01.004

Huete, A. R. 1988. A soil-adjusted vegetation index, SAVI. Remote Sensing of Environment, 25, 3, 295-309. https://doi.org/10.1016/0034-4257(88)90106-X

IS 4987. 1994. Recommendations for establishing network of raingauge stations. Bureau of Indian Standards.

Kumar, D. N. 2010. Multicriterion analysis in engineering and management. PHI Learning Pvt. Ltd.

Mokhtari, E., et al. 2023. Flood risk assessment using analytical hierarchy process: Case study from the Cheliff-Ghrib watershed, Algeria. Journal of Water and Climate Change, 14, 3, 694-711.

https://doi.org/10.2166/wcc.2023.316

Ogato, G. S., et al. 2020. GIS-based multicriteria analysis of flooding hazard and risk in Ambo Town, Ethiopia. Journal of Hydrology: Regional Studies, 27. https://doi.org/10.1016/j.ejrh.2019.100659

Parsian, S., et al. 2021. Flood hazard mapping using fuzzy logic, AHP, and multi-source geospatial datasets. Remote Sensing, 13, 23. https://doi.org/10.3390/rs13234761

Pradhan-Salike, I. and Pokharel, J. R. 2017. Impact of urbanization and climate change on urban flooding: Case of Kathmandu Valley. Journal of Natural Resources and Development, 7, 56-66. https://doi.org/10.5027/jnrd.v7i0.07

S4W-Nepal. 2023. Hanumante River flood 2023 Facebook Post. https://www.facebook.com/S4WNepal/posts/pfbid02agDQHYFdibgHN4qYfZAc4pLxvxJJwRXDkmydvYTTqfqf59ur6jBYj2ctaLXcVfw4l

Saaty, T. L. 1977. A scaling method for priorities in hierarchical structures. Journal of Mathematical Psychology, 15, 3, 234-281. https://doi.org/10.1016/0022-2496(77)90033-5

Saaty, T. L. and Vargas, L. 2001. Models, methods, concepts and applications of the analytic hierarchy process. https://doi.org/10.1007/978-1-4614-3597-6

Saha, A., et al. 2018. Assessment and impact of soil moisture index in agricultural drought estimation using remote sensing and GIS techniques. In ECWS-3 Proceedings, MDPI, 2. https://doi.org/10.3390/ecws-3-05802

Shrestha, B. R., Rai, R. K. and Marasini, S. 2020. Review of flood hazards studies in Nepal. The Geographic Base, 7, 24-32. https://doi.org/10.3126/tgb.v7i0.34266

Swain, K. C., Singha, C. and Nayak, L. 2020. Flood susceptibility mapping through the GIS-AHP technique using the cloud. ISPRS International Journal of Geo-Information, 9, 12. https://doi.org/10.3390/ijgi9120720

Winsemius, H., & Ward, P. 2015. Aqueduct global flood risk country rankings. World Resources Institute.